Concanavalin A-Rose Bengal bioconjugate for targeted Gram-negative antimicrobial photodynamic therapy

Journal of Photochemistry & Photobiology, B: Biology xxx (xxxx) xxx-xxx

Contents lists available at ScienceDirect

Journal of Photochemistry & Photobiology, B: Biology

journal homepage: http://ees.elsevier.com

Concanavalin A-Rose Bengal bioconjugate for targeted Gram-negative antimicrobial photodynamic therapy

Andrea Cantelli [a], Francesca Piro [b], Pietro Pecchini [a], Matteo Di Giosia [a], Alberto Danielli [b,*], Matteo Calvaresi [a,*]

[a] Dipartimento di Chimica "Giacomo Ciamician", Alma Mater Studiorum – Università di Bologna, Via Francesco Selmi 2, 40126 Bologna, Italy
[b] Dipartimento di Farmacia e Biotecnologie, Alma Mater Studiorum - Università di Bologna, via Francesco Selmi 2, 40126 Bologna, Italy

ARTICLE INFO

Keywords
Antimicrobial photodynamic therapy
Bioconjugation
Gram-negative bacteria targeting
Concanavalin A
Rose Bengal
Carbohydrate-lectin recognition process

ABSTRACT

Photodynamic therapy (PDT) is considered a very promising therapeutic modality for antimicrobial therapy. Although several studies have demonstrated that Gram-positive bacteria are very sensitive to PDT, Gram-negative bacteria are more resistant to photodynamic action. This difference is due to a different cell wall structure. Gram-negative bacteria have an outer cell membrane containing lipopolysaccharides (LPS) that hinder the binding of photosensitizer molecules, protecting the bacterial cells from chemical attacks. Combination of the lipopolysaccharides-binding activity of Concanavalin A (ConA) with the photodynamic properties of Rose Bengal (RB) holds the potential of an innovative protein platform for targeted photodynamic therapy against Gram-negative bacteria. A ConA-RB bioconjugate was synthesized and characterized. Approximately 2.4 RB molecules were conjugated per ConA monomer. The conjugation of RB to ConA determines a decrease of the singlet oxygen generation and an increase of superoxide and peroxide production. The photokilling efficacy of the ConA-RB bioconjugate was demonstrated in a planktonic culture of *E. coli*. Irradiation with white light from a LED lamp produced a dose-dependent photokilling of bacteria. ConA-RB conjugates exhibited a consistent improvement over RB (up to 117-fold). The improved uptake of the photosensitizer explains the enhanced PDT effect accompanying increased membrane damages induced by the ConA-RB conjugate. The approach can be readily generalized (i) using different photo/sonosensitizers, (ii) to target other pathogens characterized by cell membranes containing lipopolysaccharides (LPS).

1. Introduction

Photodynamic therapy (PDT) is considered a very promising approach for antimicrobial therapy [1–3]. PDT is a therapeutic modality used in the clinical practice of several types of cancer [4] and dermatological diseases [5]. A variety of photosensitizers (PS) [6] have already received regulatory approval or are under clinical trial, for the therapy of several diseases worldwide [7]. In PDT the PS are accumulated in the target cells. The activation of the PS by harmless visible light, convert molecular oxygen in reactive oxygen species (ROS). The generation of ROS in the target cells induce cellular damages that can lead, ultimately, to cell death. Compared to conventional antimicrobial therapies, PDT presents several advantages: [8–14] i) elimination of antibiotic-resistant microorganisms, ii) therapeutic modality (physical treatment) that does not lead to bacterial resistance, iii) redoubled selectivity (cytotoxic effects only where both sensitizers and light are delivered concomitantly), iv) immediate onset of action. Several studies have demonstrated that Gram-positive bacteria are very sensitive to PDT; Gram-negative bacteria, by contrast, are more resistant to photodynamic action [15]. This difference is due to a different cell wall structure. Gram-positive bacteria readily take up PS and are easily killed by PDT treatment. Gram-negative bacteria have an outer cell membrane containing lipopolysaccharides (LPS) that impede the binding of PS molecules, protecting the bacterial cells from chemical attacks. Different methodologies were developed to improve PS penetration in Gram-negative bacteria [8,16,17], such as the use of specific PS carriers [18], conjugation with targeting moieties [19–21], the choice of cationic PS [22] or the use of outer membrane perturbing agents [23]. Here we show a new strategy able to transform LPS [24,25], and the Gram-negative bacterial outer membrane in an Achilles heel [26]. LPS are a class of glycoconjugates consisting in i) a hydrophobic lipid domain anchored in the membrane (lipid A), ii) a polysaccharide domain made of repeating oligosaccharide units of two to eight sugar residues (O-antigen) and iii) a oligosaccharide chain connecting the lipid A and the O-antigen domains (Core-OS).

The surface polysaccharide carbohydrate of LPS, that occupy about 75% of the bacterial surface area, are recognized by lectins.

* Corresponding authors.
E-mail address: matteo.calvaresi3@unibo.it (M. Calvaresi)

https://doi.org/10.1016/j.jphotobiol.2020.111852
Received 30 October 2019; Received in revised form 18 Febraury 2020; Accepted 12 March 2020
Available online xxx
1011-1344/

Lectins are a large family of proteins that selectively bind to the saccharide components of LPS. Concanavalin A (ConA), extracted from Jack bean (*Canavalian ensiformis*) is the most widely used and well-characterized lectin. ConA binds specifically to mannosyl and glucosyl residues of polysaccharides and it can interact with bacterial surface LPS with different binding ability [27–30]. ConA has been used for specific recognition of *E. coli* surface [31–33] or for saccharides detection in *Candida albicans* [34]. Conjugation of molecules to ConA does not alter the specific binding properties of the protein. The combination of the recognition ability of ConA with the photodynamic action of Rose Bengal (RB), a prototypical PS approved for PDT, can generate an innovative protein platform for targeted Gram-negative antimicrobial PDT. RB is a halogenated dye, belonging to the xanthene class of dyes. RB has been widely used in antimicrobial photodynamic therapy [35–37]. RB is highly active against Gram-positive bacteria, while its activity against Gram-negative bacteria is low. The conjugation of RB to ConA can promote significant improvements in RB Gram-negative antimicrobial PDT killing efficiency, by increasing its local concentration on the surface of Gram-negative bacteria (Fig. 1).

2. Experimental Details

2.1. Materials

Concanavalin A from Jack bean (*Canavalia ensiformis*) Type IV lyophilized powder (ConA) (Cat. No. C2010), Rose Bengal (RB) disodium salt (Cat. No. 330000), N-Hydroxysulfosuccinimide sodium salt (Sulfo-NHS) (Cat. No. 56485), N-(3-Dimethylaminopropyl)-N′-ethylcarbodiimide hydrochloride (EDC) (Cat. No. 03450), 10-Acetyl-3,7-dihydroxyphenoxazine (Amplex Red) (Cat. No. 90101), Type VI-A Peroxidase from horseradish lyophilized powder (HRP) (Cat. no. P6782), Hydrogen Peroxide Solution 30% (*w*/w) (Cat. No. 31642-M), 9,10-Anthracenediyl-bis(methylene)dimalonic acid (ABMDMA) (Cat. No. 75068), Nitrotetrazolium Blue chloride (NBT) (Cat. no. N6639), Terephthalic acid (Cat. no. 185361), 4′,6-Diamidino-2-phenylindole dihydrochloride (DAPI) (Cat. No. D9542), Propidium iodide (PI) (Cat. No. P4170) and 14 KD cellulose dialysis tubing (Cat. No. D9652) from Sigma Aldrich (Merck). milli-Q water was used for the preparation of all the aqueous solutions.

2.2. Instrumentation

Fluorescence measures for peroxides quantification and absorbance measures for the bacteria growth recovery were performed using a Perkin Elmer EnSpire® Multimode Plate Reader. Absorption spectra were recorded using a Cary 60 UV–Vis spectrophotometer (Agilent).

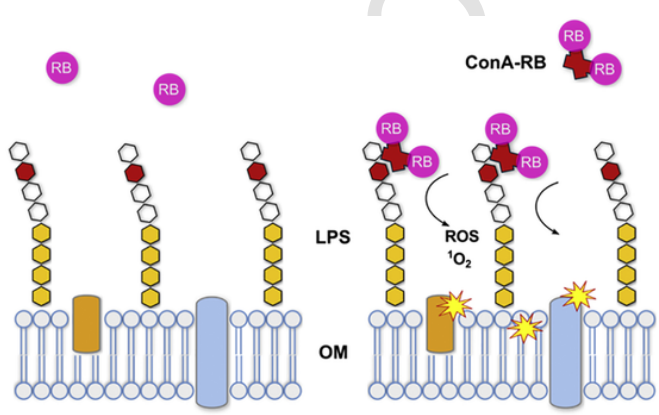

Fig. 1. Schematic representation of the ConA-RB bioconjugate activity against Gram-negative bacteria.

2.3. ConA-RB Synthesis

Rose Bengal disodium salt was dissolved in DMSO to obtain a concentration 10 mM, then solid EDC and Sulfo-NHS were added under stirring, to obtain a final concentration of 27.5 mM and 15 mM respectively. After 5 h this solution was mixed, under vigorous stirring, to Concanavalin A 0.05 mM in sodium carbonate buffer 100 mM (pH 9) with a ten-fold excess of activated RB (concentration 0.5 mM). The reaction was incubated overnight under mild stirring condition.

2.4. ConA-BR Purification

Once the cross-linking reaction was completed, the ConA-RB bioconjugate was purified by dialysis. Unreacted RB and small molecular weight byproducts of the crosslinking reaction were removed by dialysis in sodium carbonate buffer 10 mM (pH 9) using a membrane with a 14,000 KD cut off. Dialysis was repeated until the UV–vis signal at 550 nm typical of the RB disappeared completely from the dialyzing solution. ConA-RB synthesis and purification are carried out at room temperature.

2.5. ABMDMA Singlet Oxygen Assay

Isoabsorbing solutions at 555 nm of RB and ConA-RB were prepared. ABMDMA was added to the solutions to reach a final concentration of 15 μM of the sensitizer and 25 μM of ABMDMA. The solutions were stirred vigorously to ensure air saturation. The solutions were irradiated at 555 nm and the bleaching of the absorption band of ABMDMA at 401 nm was monitored.

The singlet oxygen quantum yield (ΦΔ) was determined using Rose Bengal (RB) as the reference with a yield of 0.76 in PBS.

The ΦΔ of ConA-RB was calculated by the following equation

$$\Phi_{\Delta}^{S} = \frac{k_S}{k_R} \times \Phi_{\Delta}^{R}$$

where K is the slope of the photodegradation rate of ABMDMA, S represents the sample (ConA-RB), R means the reference (RB), and is $\Phi_{\Delta}{}^{R}$ the ΦΔ of the reference (RB).

2.6. Amplex Red Peroxides Quantification

1 mL of phosphate buffered saline 50 mM pH 7.4 was added to 10 μL of Amplex Red 50 mM in DMSO. Then 10 μL of HRP 0.4 mg/mL in PBS 50 mM pH 7.4 was added to the Amplex Red solution to obtain the final working solution. 90 μL of the solutions under investigation, containing different concentrations (0.025 μM, 0.05 μM, 0.25 μM, 0.5 μM, 2.5 μM and 5 μM) of RB or ConA-RB in PBS 50 mM pH 7.4, isoabsorbing in the visible range, were irradiated for 45 min with visible light (white LED Valex 30 W lamp at 30 cm distance from the cell-plate, irradiation power density on the cell plate = 2 mW/cm^2; measured with the photo-radiometer Delta Ohm LP 471 RAD), on microtiter plates and 10 μL of Amplex Red working solution was added to each sample immediately after irradiation. Solutions were incubated 30 min at room temperature and the absorbance of the samples is read at 560 nm. The absorbance values were converted to the concentration of H_2O_2 generated upon irradiation, using a calibration curve generated using standard solutions of H_2O_2.

2.7. Nitroblue Tetrazolium (NBT) Assay to Determine the Production of Superoxide Anion

3 ml of isoabsorbing solutions of RB and ConA-RB (2.5 μM) in PBS 50 mM pH 7.4 were prepared. NBT was added to the solutions to reach a final concentration of 0.24 mM. Control solutions of NBT in milli-Q water and NBT in ConA were also prepared. The solutions were irradiated for 45 min with visible light (white LED Valex 30 W lamp at 30 cm distance from the cuvette, irradiation power density on the cell plate = 2 mW/cm^2; measured with the photo-radiometer Delta Ohm LP 471 RAD).

A dark blue insoluble precipitate of NBT-formazan is generated upon reaction of NBT with superoxide anion radical. The NBT-formazan product is extracted, dissolved in isopropanol/HCl solution and the absorbance is read at 490 nm. The absorbance values were converted to the concentration of superoxide anion generated upon irradiation, using the molar extinction coefficient of the produced NBT-formazan at 490 nm (100.000 M^{-1} cm^{-1}) [38].

2.8. Terephthalate (TPA) Assay to Determine the Production of Hydroxyl Radical

A 200 mM stock solution of terephthalic acid (TPA) was prepared using NaOH. 2.5 μM solutions of RB and ConA-RB in PBS 50 mM pH 7.4 were prepared. TPA was added to the solutions to reach a final concentration of 500 μM. The solutions were irradiated at 554 nm where RB and ConA-RB are isoabsorbing. The changes in fluorescence at 425 nm (excitation 315 nm), due to the production of 2-hydroxyterephthalate (HTPA), was measured using a Edinburgh Analytical Instruments FLS920 spectrofluorometer. All fluorescence measurements were carried out at room temperature.

2.9. Photodynamic Antimicrobial Activity Assay

The antimicrobial activity of ConA-adducts was tested on *E. coli* (strain DH5α) during exponential growth. Bacteria were resuspended in PBS 1× to obtain a final concentration of 2·10^6 cfu/ml in each well of a 96-well microtiter plate. Different concentrations of RB and ConA-RB were used, in a sensitizer concentration range between 5 and 0.025 μM. The plate with bacteria and photosensitizers was incubated for 30 min in the dark and subsequently irradiated for 45 min with white LED lamp producing 2 W/cm^2 at the cell plate, at room temperature. These conditions were optimized to provide the maximum non-lethal light fluency on untreated DH5α control cultures.

Control plates were kept in the dark at room temperature. After irradiation, bacteria were inoculated in LB broth (1:10 dilution) in a new microtiterplate. The plate was kept at 37 °C in an EnSpire multimode plate reader (PerkinElmer) and the recovery of growth was measured reading the increase of absorbance (600 nm) every 10 min for 15 h. The antimicrobial photocatalytic activity of adducts and controls was inferred by measuring the delay in time (=number of generations) needed to reach the onset of the exponential phase of growth (normalized A_{600} = 0.125), relative to the control samples kept in the dark.

2.10. Photosensitizer Uptake by Bacteria

2·10^5 bacteria grown in LB to exponential phase were pelleted by centrifugation, washed once in 1×PBS and then resuspended in 200 μL 1×PBS containing RB or the ConA-RB adduct (both at 2.5 μM sensitizer). After 30-min incubation in the dark, bacteria were pelleted and the supernatant, containing unbound RB or ConA-RB, was collected. Bacterial pellets were then extensively washed 3 times and resuspended in 1X PBS. All fractions were collected for fluorescence readout and read in an EnSpire multimode plate reader (PerkinElmer; 560/575 nm excitation/emission).

2.11. Membrane Damage Assay

A fluorimetric permabilization assay was used to investigate the light-dependent damage induced by RB and ConA-RB on the bacterial membrane. This assay is based on Propidium Iodide (PI), a widely used DNA intercalating fluorescent stain unable to permeate intact, undamaged cell membranes. Briefly, 5·10^8 bacterial cells grown to late exponential phase (A_{600} = 0.9) were pelleted, and resuspended in 1× PBS containing the ConA-RB adduct or RB alone (2.5 μM sensitizer for both) the wells of two microtiter plates. The first was irradiated as previously described, while the second was kept in the dark (control). Following irradiation, bacteria were pelleted and cross-linked for 5 min in 2% formaldehyde 1× PBS to fix the cells. The reaction was then blocked with 125 mM glycine for 10 min. After two rounds of washing in 1× PBS, bacteria were stained in a solution containing 2 μg/ml 4′,6-diamidino-2-phenylindole (DAPI) and 0.3 μg/ml PI in 1× PBS. After a last washing step in PBS, the fluoresence signal of PI (535/617 nm) and DAPI (358/461 nm) was recorder in a plate reader. DAPI was used to normalize the PI fluorescent signal since it similarly stains the DNA of both permeabilized and non-permeabilized cells. The permabilization index, defined as the PI/DAPI signal ratio, was normalized to the control samples kept in the dark (n = 6).

3. Results and Discussion

3.1. Synthesis and Purification of ConA-RB Bioconjugate

The novel ConA-RB bioconjugate was synthesized via EDC/NHS cross coupling reaction between the carboxylic-acid group of RB and amino acid amine groups of ConA (Fig. 2). Once the cross-linking reactions were completed the ConA-RB bioconjugate was purified by dialysis.

3.2. Spectroscopic Characterization of ConA-RB Bioconjugate

Absorption spectra of the purified ConA-RB bioconjugate displayed the diagnostic peaks, characteristic of RB (Fig. 3A).

The absorbance peak of ConA-RB shifted to 560 nm (the typical absorbance of RB is at 549 nm) and became broader following conjugation with ConA (Fig. 3B). These changes in the absorption spectra confirmed that RB was attached to ConA [39–41].. Considering that the initial concentration of ConA is 50 μM, the molar extinction coefficient of RB at 550 nm is 90,000 M^{-1} cm^{-1} and the absorbance of the purified ConA-RB is 1,08 (Fig. 3a, spectrum obtained with a 1:10 diluition), approximately 2.4 RB molecules were conjugated per ConA monomer.

3.3. ROS Generation Ability of ConA-RB Bioconjugate

Upon light absorption, PS can produce ROS via two different pathways [42]. The singlet excited state of the photosensitizer, initially formed, convert to a long-lived triplet state through the intersystem crossing. In type I mechanism, a radical species is generated by electron transfer from (or to) the excited state of the photosensitizer. This radical species readily reacts with molecular oxygen forming different reactive oxygen species (ROS). In type II mechanism, the transfer of energy from the excited triplet state of the photosensitizer to ground-state molecular oxygen ($^3O_2$) generates singlet oxygen ($^1O_2$).

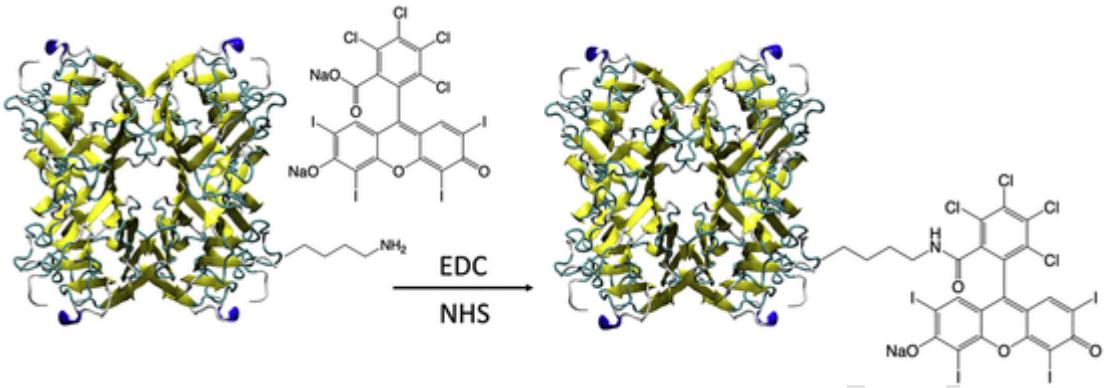

Fig. 2. Conjugation of RB to Concanavalin A.

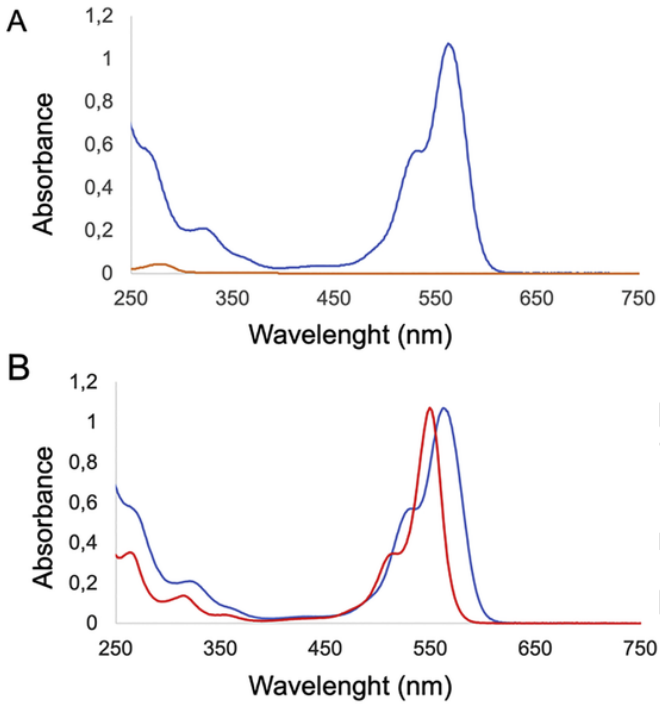

Fig. 3. A) Absorption spectra of ConA (orange line) and ConA-RB (blue line). B) Normalized absorption spectra of RB (red line) and ConA-RB (blue line). (For interpretation of the references to colour in this figure legend, the reader is referred to the web version of this article.)

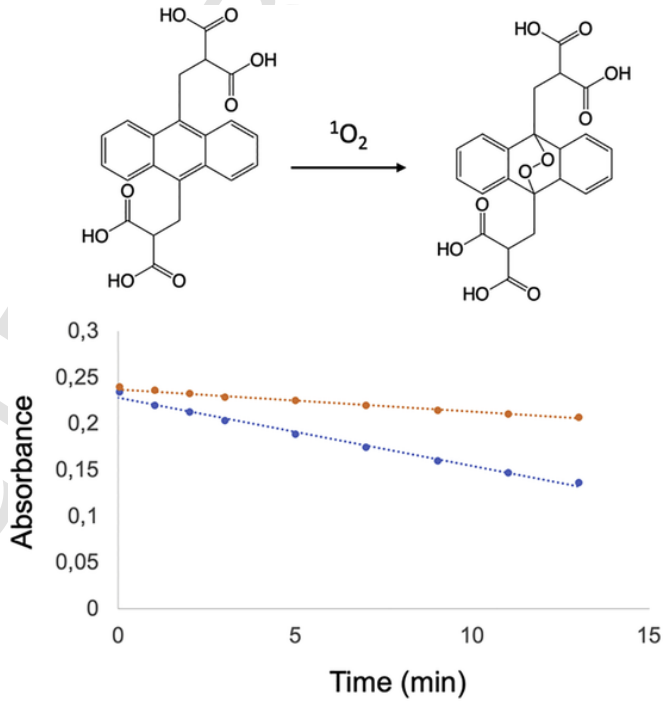

Fig. 4. Decrease of ABMDMA absorbance vs. irradiation time under a 555 nm irradiation for RB (blue line) and ConA-RB bioconjugate (orange line). (For interpretation of the references to colour in this figure legend, the reader is referred to the web version of this article.)

The presence of the two mechanisms can be easily verified by spectrofluorimetric measurements

RB is a known type II photosensitizer and it acts by a type II mechanism, involving $^1O_2$ generation. Conjugated RB can work with different mechanisms. The amount of $^1O_2$ generated during visible light irradiation by RB and ConA-RB was therefore measured.

We used as $^1O_2$ detector 9,10-anthracenediyl-bis(methylene)dimalonic acid (ABMDMA). The disodium salt of ABMDMA reacts with $^1O_2$ to give an endoperoxide (Fig. 4). This reaction is detected by the bleaching of ABMDMA. From the decline of the absorbance at 401 nm, the generation of $^1O_2$ upon irradiation is determined (see ABMDMA singlet oxygen assay section in Experimental details). The singlet oxygen quantum yield (Φ_Δ) of ConA-RB bioconjugates was calculated ($\Phi_{\Delta\text{-ConA-RB}} = 0.24$) using free Rose Bengal (RB) as reference ($\Phi_{\Delta\text{-RB}} = 0.76$) [43]. The results indicated that the ConA-RB bioconjugates generate approximately one-third $^1O_2$ with respect to free RB (Fig. 4).

The ability of RB and ConA-RB to generate peroxides, upon irradiation with visible light, was evaluated using the Amplex Red (*N*-acetyl-3,7-dihydroxyphenoxazine) assay. The colorless, non-fluorescent Amplex Red, catalyzed by horseradish peroxidase (HRP), reacts stoichiometrically with peroxides, to form colored, fluorescent resorufin (Fig. 5),

Different concentrations of RB and ConA-RB in PBS were tested (Fig. 5).

The concentration of the produced peroxides is calculated as the difference of resorufin generated by the irradiation of RB and ConA-RB and that of the references, i.e., isoabsorbing RB and ConA-RB solutions, kept in the dark. ConA-RB showed an improved ability to generate peroxides with respect to free RB.

Nitroblue tetrazolium (NBT) assay is used to determine the production of superoxide anion radical.

The NBT test evaluate the formation of the superoxide anion radicals by quantifying the production of dark blue NBT-formazan precipitate, generated by the reduction of the yellow colored NBT by su-

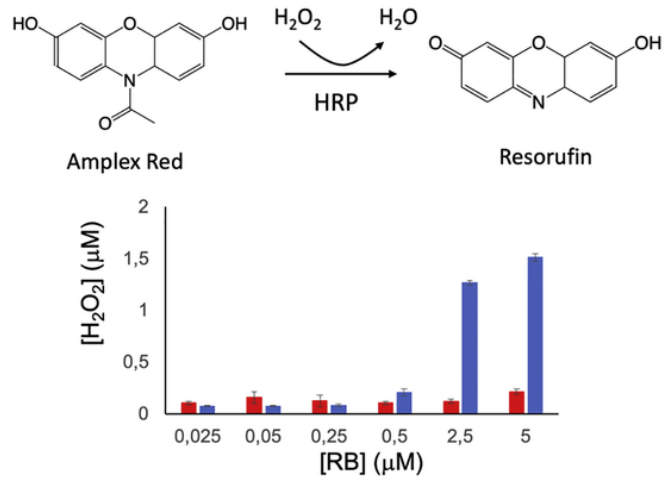

Fig. 5. Generation of peroxides during visible light irradiation, using different concentrations of RB (red) and ConA-RB (blue). (For interpretation of the references to colour in this figure legend, the reader is referred to the web version of this article.)

peroxide anion radical (Fig. 6). ConA-RB showed a 10-fold ability to generate superoxide anion radicals with respect to free RB.

The production of hydroxyl radicals, upon irradiation of RB and ConA-RB was investigated using the TPA assay. The colorless, non-fluorescent TPA selectively reacts with hydroxyl radicals to form the strongly fluorescent 2-hydroxyterephthalate (HTPA, Fig. 7). From the increase of the fluorescence at 425 nm, generated by the production of HTPA, the rates of hydroxyl radical generation, upon irradiation, by RB and ConA-RB are determined.

The performances of ConA-RB and RB are exactly the same, suggesting that the conjugation of RB with ConA does not have any effect in the production of hydroxyl radicals upon irradiation.

RB is a type II photosensitizer and generates mainly $^1O_2$. A sacrificial electron donor is generally required to activate the type I mechanism [44]. ConA-RB hybrid does not need any external electron donors because the protein residues of ConA can participate directly in the electron transfer reactions. This means that the type I mechanism is self-activated in the ConA-RB hybrid, due to the presence of the protein itself [45,46]. Electron-rich environments increase photoactivation switch from type II to type I mechanisms [47], which significantly increases the generation of superoxide anion radical (electron transfer process) over singlet oxygen production (energy transfer process).

In the ConA-RB hybrid type I mechanism is promoted by the presence of protein electron donors, giving promptly superoxide anion radical. Superoxide then can react with itself to produce hydrogen peroxide and oxygen (superoxide radical dismutation). RB conjugation does not have any effect on the production of hydroxyl radicals.

In summary, ConA-RB showed an improved ability to generate ROS by Type I mechanism with respect to free RB. The conjugation of RB to ConA determines a decrease of the $^1O_2$ generation and an increase of peroxide production, via superoxide radical anion formation, disfavouring type II mechanism and enhancing type I mechanism.

3.4. Photokilling attivity of RB and ConA-RB Bioconjugate in a Planktonic Culture of E. coli

To assess if ConA-RB is able to target Gram-negative bacteria, the viability of *E. coli* in planktonic culture, after photodynamic treatment with ConA-RB or RB alone, was measured. The antimicrobial activity was tested on strain DH5α during the exponential growth phase. Different concentrations of RB and ConA-RB conjugates were used, in a range between 5 and 0.025 μM of sensitizer. Light alone without photosensitizers (RB and ConA-RB) and photosensitizers (RB and ConA-RB) without irradiation (dark control) were included as negative controls. Microtiters plates with bacteria and photosensitizers were incubated for 30 min in dark conditions and subsequently irradiated for 45 min with a white LED lamp at room temperature (2 mW/cm^2). Control plates were kept in the dark at room temperature. After irradiation, bacteria were inoculated in LB and the recovery of growth was measured at regular time intervals, in order to measure the delay. Illumination with white light from a LED lamp produced a dose-dependent photokilling of bacteria (Fig. 8).

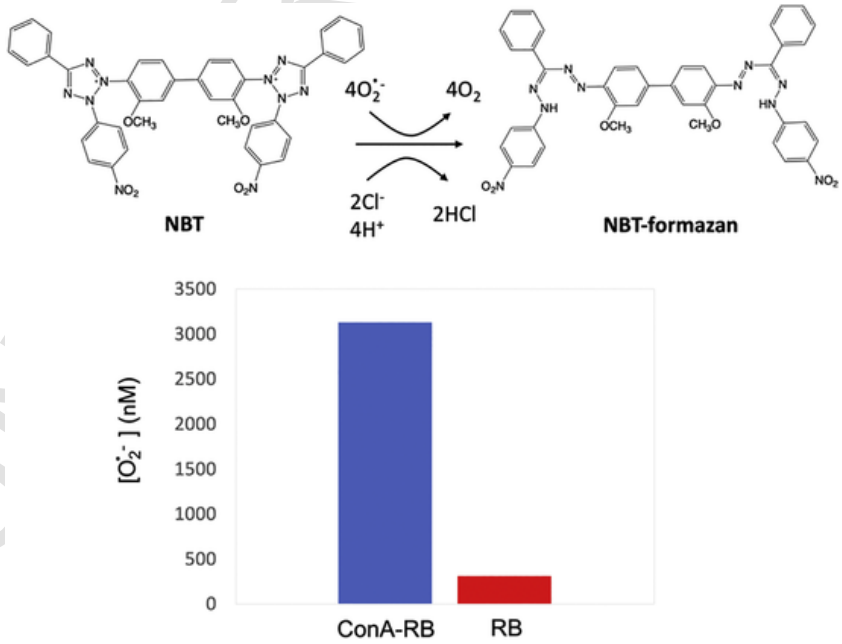

Fig. 6. Generation of superoxide anion radical during visible light irradiation, using 2.5 μM of RB (red) and ConA-RB (blue). (For interpretation of the references to colour in this figure legend, the reader is referred to the web version of this article.)

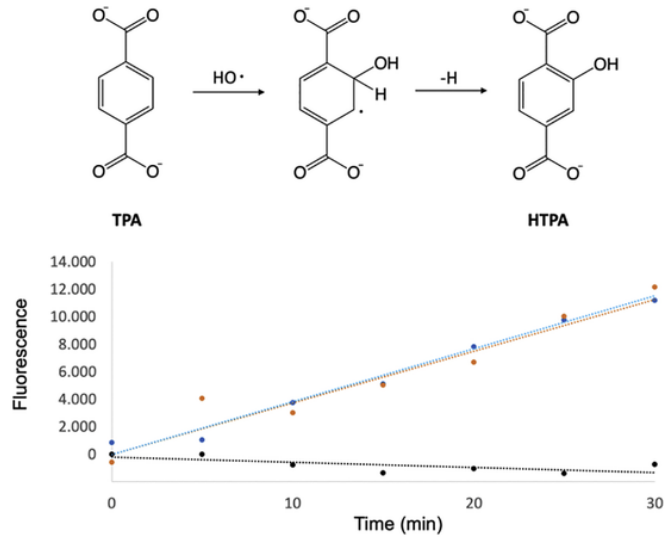

Fig. 7. Increase of HTPA fluorescence (425 nm) vs. irradiation time under a 325 nm irradiation for RB (blue line); ConA-RB bioconjugate (orange line) and control (TPA in milli-Q water). (For interpretation of the references to colour in this figure legend, the reader is referred to the web version of this article.)

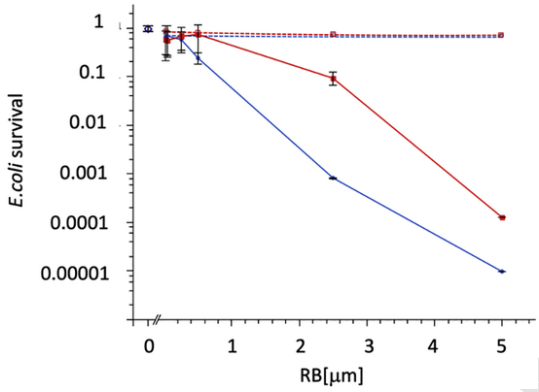

Fig. 8. Photoinactivation of *E.coli* DH5α. Cells were incubated with different concentrations of RB (red lines) and ConA-RB conjugate (blue lines), in a range betwen 5 to 0.025 μM followed by irradiation. Solid line (light condition), dashed line (dark condition). At 0 the effect of the light alone without photosensitizers. The values shown are means of five independent experiments, and bars are the standard error of the mean. (For interpretation of the references to colour in this figure legend, the reader is referred to the web version of this article.)

At very low RB concentration (0.025–0.25 μM) no photodynamic activity was observed, probably because the generation of ROS is too low to kill the bacteria. At 0.5 μM free RB failed to elicit any significant effect, while ConA-RB conjugate killed 57% of the bacteria. At 2.5 and 5 μM photodynamic antimicrobial activity was observed for both RB and ConA-RB. However, ConA-RB conjugates exhibited a consistent improvement over RB (117- and 13-fold, respectively). These results can be explained by the selective recognition of LPS by ConA, that contributes significantly to the enhanced PDT effect showed by the ConA-RB conjugate.

3.5. Uptake of RB and ConA-RB Bioconjugate

To further investigate the enhanced photokilling effect exerted by the ConA-RB conjugate we evaluated the bacterial uptake of RB and ConA-RB.

Bacteria were incubated with RB or ConA-RB adduct (2.5 μM) for 30 min. Then the bacteria were pelleted and the supernatant, containing the unbound RB or ConA-RB, was collected. After extensive washing, the bacterial cells were harvested and subjected to fluorescence readout to measure the bound fraction of adducts, together with the supernatant (Fig. 9).

The binding of ConA-RB bioconjugate to the bacterial membrane of *E.coli* is 4.5 fold higher than RB alone, demonstrating the crucial role of ConA bioconjugation, that improves the binding of the photosensitizer to the external membrane of the bacteria by the selective recognition of LPS. Accordingly, the increase in local PS concentration explains the enhanced PDT effect showed by the ConA-RB conjugate.

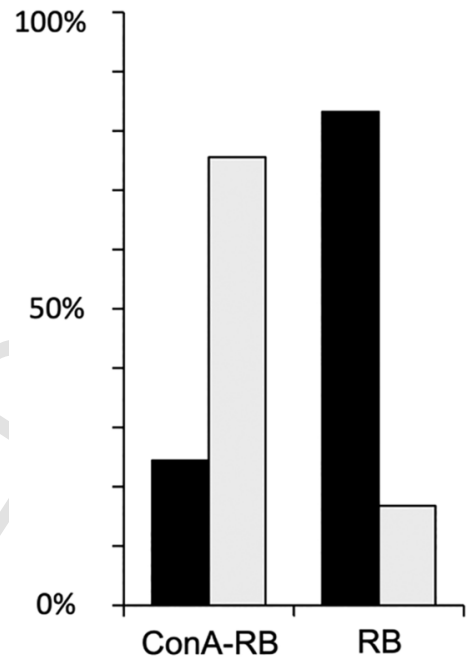

Fig. 9. RB and ConA-RB adduct uptake. PS fluorescence in unbound (black bars) and bacterial bound fractions (grey bars). Percent values over the sum of fluorescence signals in both fractions.

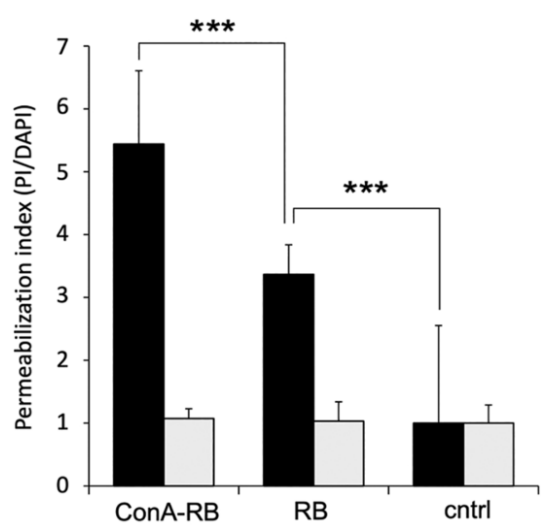

Fig. 10. Quantification of PDT-induced membrane permeabilization. The uptake of PI, a DNA intercalating fluorescent stain unable to cross intact membranes, was normalized to DAPI. Permeabilization assays were carried out after light irradiation (black bars) or under dark conditions (grey bars). The permeabilization index of untreated control samples kept in the dark was set to 1. Error bars represent the standard deviation ($n = 6$). Statistical significance was inferred using Student's *t*-test (***, $p < .005$).

3.6. Effect of the PDT Treatment on the Bacterial Membrane Integrity

The structure of biological membranes is strongly affected by oxidative stress. The *E.coli* membrane integrity after the PDT treatment was assessed using a mixture of two dyes: 4′,6-diamidino-2-phenylindole (DAPI) and propidium iodide, (PI). DAPI stains both viable and nonviable bacteria, regardless of their physiological status, while PI only enters in bacteria with damaged membranes.

The measure of the permeabilization index (PI/DAPI normalized fluorescence) demonstrates that the PDT treatment provokes significant impairment of membrane permeability only in the presence of the photosensitizer and light (Fig. 10). Importantly, the ConA-RB conjugate appears to elicit stronger membrane damage than RB alone, in accordance with its increased uptake in *E.coli* cells.

4. Conclusions

The intrinsic biocompatibility of peptides and proteins makes them promising candidates for biomedical applications, especially for PDT [48–52]. Use of targeting delivery system is the most efficient strategy to enhance the antimicrobial [53,54] and anticancer efficacy of PDT [55]. Here we demonstrated how the conjugation of a model photosensitizer, RB, to a protein characterized by lipopolysaccharides-binding activity, ConA, leads to a more effective targeting of RB to Gram-negative negative bacteria. This strategy is based on the high specificity of carbohydrate-lectin recognition process [56,57]. Glycoconjugates are used to target bacterial lectins [20,58], here we reversed the process and we used a lectin, namely concanavalin A, to recognize specific glycoconjugates, i. e. lipopolysaccharides, present on the surface of Gram-negative bacteria.

Conjugation of RB with ConA increases i) the uptake of the photosensitizer, ii) its photokilling efficacy and iii) membrane damages after PDT treatment. A modulation between type I and type II mechanisms in the ROS generation is exerted by the protein conjugation.

Even if the current set of experiments is not sufficient to validate ConA-RB bioconjugates as a novel targeted-photosensitizer with clinical significance, they may pave the way to additional in-vivo PK/PD, therapeutic and toxicity studies needed for their translational application.

The developed procedure of conjugation of RB to ConA is general and may be used for any photosensitizer in targeted Gram-negative antimicrobial photodynamic therapy, improving the therapeutic efficiency of PDT.

Declaration of Competing Interest

The authors declare that they have no known competing financial interests or personal relationships that could have appeared to influence the work reported in this paper.

References

[1] F Vatansever, W C M A de Melo, P Avci, D Vecchio, M Sadasivam, A Gupta, R Chandran, M Karimi, N A Parizotto, R Yin, G P Tegos, M R Hamblin, Antimicrobial strategies centered around reactive oxygen species - bactericidal antibiotics, photodynamic therapy, and beyond, FEMS Microbiol. Rev. 37 (2013) 955–989.

[2] G Jori, C Fabris, M Soncin, S Ferro, O Coppellotti, D Dei, L Fantetti, G Chiti, G Roncucci, Photodynamic therapy in the treatment of microbial infections: basic principles and perspective applications, Lasers Surg. Med. 38 (2006) 468–481.

[3] M Q Mesquita, C J Dias, P M S Neves, A Almeida, M A F Faustino, Revisiting current photoactive materials for antimicrobial photodynamic therapy, Molecules 23 (2018) 2422.

[4] P Agostinis, K Berg, K A Cengel, T H Foster, A W Girotti, S O Gollnick, S M Hahn, M R Hamblin, A Juzeniene, D Kessel, M Korbelik, J Moan, P Mroz, D Nowis, J Piette, B C Wilson, J Golab, Photodynamic therapy of cancer: an update, CA Cancer J. Clin. 61 (2011) 250–281.

[5] P Babilas, S Schreml, M Landthaler, R M Szeimies, Photodynamic therapy in dermatology: state-of-the-art, Photodermatol. Photoimmunol. Photomed. 26 (2010) 118–132.

[6] M Lan, S Zhao, W Liu, C S Lee, W Zhang, P Wang, Photosensitizers for photodynamic therapy, Adv. Healthc. Mater. 8 (2019) 1900132.

[7] G B Kharkwal, S K Sharma, Y Y Huang, T Dai, M R Hamblin, Photodynamic therapy for infections: clinical applications, Lasers Surg. Med. 43 (2011) 755–767.

[8] Y Liu, R Qin, S A J Zaat, E Breukink, M Heger, Antibacterial photodynamic therapy: overview of a promising approach to fight antibiotic-resistant bacterial infections, J. Clin. Transl. Res. 1 (2015) 140–167.

[9] M R Hamblin, Antimicrobial photodynamic inactivation: a bright new technique to kill resistant microbes, Curr. Opin. Microbiol. 33 (2016) 67–73.

[10] A Tavares, C M B Carvalho, M A Faustino, P M S Neves, J P C Tomé, A C Tomé, J A S Cavaleiro, Â Cunha, N C M Gomes, E Alves, A Almeida, Antimicrobial photodynamic therapy: Study of bacterial recovery viability and potential development of resistance after treatment, Mar. Drugs. 8 (2010) 91–105.

[11] F Cieplik, D Deng, W Crielaard, W Buchalla, E Hellwig, A Al-Ahmad, T Maisch, Antimicrobial photodynamic therapy–what we know and what we don't, Crit. Rev. Microbiol. 44 (2018) 571–589.

[12] M Wainwright, Photodynamic antimicrobial chemotherapy (PACT), J. Antimicrob. Chemother. 42 (1998) 13–28.

[13] T H Michael Hamblin, Photodynamic therapy: a new antimicrobial approach to infectious disease, Photochem. Photobiol. 3 (2011) 436–450.

[14] Z M Marković, S P Jovanović, P Z Mašković, M Danko, M Mičušík, V B Pavlović, D D Milivojević, A Kleinová, Z Špitalský, B M Todorović Marković, Photo-induced antibacterial activity of four graphene based nanomaterials on a wide range of bacteria, RSC Adv. 8 (2018) 31337–31347.

[15] Z Malik, H Ladan, Y Nitzan, Photodynamic inactivation of gram-negative bacteria: problems and possible solutions, J. Photochem. Photobiol. B Biol. 14 (1992) 262–266.

[16] T N Demidova, M R Hamblin, Photodynamic therapy targeted to pathogens, Int. J. Immunopathol. Pharmacol. 17 (2004) 245–254.

[17] M Tim, Strategies to optimize photosensitizers for photodynamic inactivation of bacteria, J. Photochem. Photobiol. B Biol. 150 (2015) 2–10.

[18] M Bhatti, T D McHugh, L Milanesi, S Tomas, Self-assembled nanoparticles as multifunctional drugs for anti-microbial therapies, Chem. Commun. 50 (2014) 7649–7651.

[19] F Le Guern, V Sol, C Ouk, P Arnoux, C Frochot, T S Ouk, Enhanced photobactericidal and targeting properties of a cationic porphyrin following the attachment of polymyxin B, Bioconjug. Chem. 28 (2017) 2493–2506.

[20] Y Zhao, Z Lu, X Dai, X Wei, Y Yu, X Chen, X Zhang, C Li, Glycomimetic-conjugated photosensitizer for specific Pseudomonas aeruginosa recognition and targeted photodynamic therapy, Bioconjug. Chem. 29 (2018) 3222–3230.

[21] V Bogoeva, L Petrova, P Kubát, Binding of palladium (II) 5, 10, 15, 20-tetrakis (4-sulfonatophenyl) porphyrin to a lectin for photosensitizer targeted delivery, J. Photochem. Photobiol. B Biol. 153 (2015) 276–280.

[22] M Wainwright, J Antczak, M Baca, C Loughran, K Meegan, Phenothiazinium photoantimicrobials with basic side chains, J. Photochem. Photobiol. B Biol. 150 (2015) 38–43.

[23] G Bertolini, F Rossi, G Valduga, G Jori, J van Lier, Photosensitizing activity of water- and lipid-soluble phthalocyanines on Escherichia coli, FEMS Microbiol. Lett. 71 (1990) 149–155.

[24] V N Tra, D H Dube, Glycans in pathogenic bacteria-potential for targeted covalent therapeutics and imaging agents, Chem. Commun. 50 (2014) 4659–4673.

[25] D H Dube, K Champasa, B Wang, Chemical tools to discover and target bacterial glycoproteins, Chem. Commun. 47 (2011) 87–101.

[26] F Liu, A S Y Ni, Y Lim, H Mohanram, S Bhattacharjya, B Xing, Lipopolysaccharide neutralizing peptide-porphyrin conjugates for effective photoinactivation and intracellular imaging of gram-negative bacteria strains, Bioconjug. Chem. 23 (2012) 1639–1647.

[27] P Ertl, S R Mikkelsen, Electrochemical biosensor array for the identification of microorganisms based on lectin - lipopolysaccharide recognition, Anal. Chem. 73 (2001) 4241–4248.

[28] Z Shen, M Huang, C Xiao, Y Zhang, X Zeng, P G Wang, Nonlabeled quartz crystal microbalance biosensor for bacterial detection using carbohydrate and lectin recognitions, Anal. Chem. 79 (2007) 2312–2319.

[29] H B Maruyama, Simplified assay for concanavalin a dependent bacterial agglutination by using cell surface mutants, Infect. Immun. 11 (1975) 1320–1324.

[30] K Baintner, B Kocsis, K Kovács, Z Péterfi, G Kökény, P Hamar, Interaction of concanavalin a with bacterial lipopolysaccharides in agarose gel, Acta Microbiol. Immunol. Hung. 58 (2011) 201–209.

[31] I Ofek, D Mirelman, N Sharon, Adherence of escherichia coli to human mucosal cells mediated by mannose receptors [13], Nature. 265 (1977) 623–625.

[32] Q Lu, S Luo, Q Cai, S Ge, C A Grimes, H Lin, Wireless, remote-query, and high sensitivity Escherichia coli O157:H7 biosensor based on the recognition action of concanavalin a, Anal. Chem. 81 (2009) 5846–5850.

[33] X Xu, Y Yuan, G Hu, X Wang, P Qi, Z Wang, Q Wang, X Wang, Y Fu, Y Li, H Yang, Exploiting pH-regulated dimer-tetramer transformation of Concanavalin a to develop colorimetric biosensing of bacteria, Sci. Rep. 7 (2017) 1–8.

[34] D P L A Tenório, C G Andrade, P E Cabral Filho, C P Sabino, I T Kato, L B Carvalho, S Alves, M S Ribeiro, A Fontes, B S Santos, CdTe quantum dots conjugated to concanavalin a as potential fluorescent molecular probes for saccharides detection in Candida albicans, J. Photochem. Photobiol. B Biol. 142 (2015) 237–243.

[35] S A Bezman, P A Burtis, T P J Izod, M A Thayer, Photodynamic inactivation of *E. coli* by rose bengal immobilized on polystyrene beads, Photochem. Photobiol. 28 (1978) 325–329.
[36] J G Banks, R G Board, J Carter, A D Dodge, The cytotoxic and photodynamic inactivation of micro-organisms by Rose Bengal, J. Appl. Bacteriol. 58 (1985) 391–400.
[37] M Schäfer, C Schmitz, R Facius, G Horneck, B Milow, K-H Funken, J Ortner, Systematic study of parameters influencing the action of rose bengal with visible light on bacterial cells: comparison between the biological effect and singlet-oxygen production, Photochem. Photobiol. 71 (2004) 514.
[38] M J Green, H A O Hill, [1] Chemistry of dioxygen, Methods Enzymol. 105 (1984) 3–22.
[39] A Shrestha, M R Hamblin, A Kishen, Characterization of a conjugate between rose bengal and chitosan for targeted antibiofilm and tissue stabilization effects as a potential treatment of infected dentin, Antimicrob. Agents Chemother. 56 (2012) 4876–4884.
[40] Ł Moczek, M Nowakowska, Novel water-soluble photosensitizers from chitosan, Biomacromolecules 8 (2007) 433–438.
[41] S Han, B W Hwang, E Y Jeon, D Jung, G H Lee, D H Keum, K S Kim, S H Yun, H J Cha, S K Hahn, Upconversion nanoparticles/hyaluronate-rose bengal conjugate complex for noninvasive photochemical tissue bonding, ACS Nano 11 (2017) 9979–9988.
[42] Y Xiong, X Tian, H W Ai, Molecular tools to generate reactive oxygen species in biological systems, Bioconjug. Chem. 30 (2019) 1297–1303.
[43] R W Redmond, J N Gamlin, A compilation of singlet oxygen yields from biologically relevant molecules, Photochem. Photobiol. 70 (1999) 391–475.
[44] P Sanchez-Cruz, F Dejesus-Andino, A E Alegria, Roles of hydrophilicities and hydrophobicities of dye and sacrificial electron donor on the photochemical pathway, J. Photochem. Photobiol. A Chem. 236 (2012) 54–60.
[45] M Di Giosia, P H H Bomans, A Bottoni, A Cantelli, G Falini, P Franchi, G Guarracino, H Friedrich, M Lucarini, F Paolucci, S Rapino, N A J M Sommerdijk, A Soldà, F Valle, F Zerbetto, M Calvaresi, Proteins as supramolecular hosts for C60: a true solution of C60 in water, Nanoscale 10 (2018) 9908–9916.
[46] M Di Giosia, D Genovese, A Cantelli, M Cingolani, E Rampazzo, G Strever, M Tavoni, N Zaccheroni, M Calvaresi, L Prodi, Synthesis and characterization of a reconstituted myoglobin-chlorin e6 adduct for theranostic applications, J. Porphyrins Phthalocyanines (2019) A-G, doi:10.1142/S108842461950202X.
[47] H Ding, H Yu, Y Dong, R Tian, G Huang, D A Boothman, B D Sumer, J Gao, Photoactivation switch from type II to type i reactions by electron-rich micelles for improved photodynamic therapy of cancer cells under hypoxia, J. Control. Release 156 (2011) 276–280.
[48] M Abbas, Q Zou, S Li, X Yan, Self-assembled peptide- and protein-based nanomaterials for antitumor photodynamic and photothermal therapy, Adv. Mater. 29 (2017) 1605021.
[49] R Chang, Q Zou, R Xing, X Yan, Peptide-based supramolecular nanodrugs as a new generation of therapeutic toolboxes against cancer, Adv. Ther. 2 (2019) 1900048.
[50] A Soldà, A Cantelli, M Di Giosia, M Montalti, F Zerbetto, S Rapino, M Calvaresi, C_{60} @lysozyme: a new photosensitizing agent for photodynamic therapy, J. Mater. Chem. B 5 (2017) 6608–6615.
[51] M Di Giosia, F Nicolini, L Ferrazzano, A Soldà, F Valle, A Cantelli, T D Marforio, A Bottoni, F Zerbetto, M Montalti, S Rapino, A Tolomelli, M Calvaresi, Stable and biocompatible monodispersion of C_{60} in water by peptides, Bioconjug. Chem. 30 (2019) 808–814, doi:10.1021/acs.bioconjchem.8b00916.
[52] F Giuntini, C M A Alonso, R W Boyle, Synthetic approaches for the conjugation of porphyrins and related macrocycles to peptides and proteins, Photochem. Photobiol. Sci. 10 (2011) 759–791.
[53] L M De Freitas, E N Lorenzón, N A Santos-Filho, L H D P Zago, M P Uliana, K T De Oliveira, E M Cilli, C R Fontana, Antimicrobial photodynamic therapy enhanced by the peptide aurein, Sci. Rep. 8 (2018) 1–15.
[54] A V Cheng, W M Wuest, Signed, sealed, delivered: conjugate and prodrug strategies as targeted delivery vectors for antibiotics, ACS Infect. Dis. 5 (2019) 816–828.
[55] J Sandland, R W Boyle, Photosensitizer antibody-drug conjugates: past, present, and future, Bioconjug. Chem. 30 (2019) 975–993.
[56] S Jayanthi, S Shanthi, B Vaseeharan, N Gopi, M Govindarajan, N S Alharbi, S Kadaikunnan, J M Khaled, G Benelli, Growth inhibition and antibiofilm potential of Ag nanoparticles coated with lectin, an arthropod immune molecule, J. Photochem. Photobiol. B Biol. 170 (2017) 208–216.
[57] C R A Cunha, C G Andrade, M I A Pereira, P E Cabral Filho, L B Carvalho, L C B B Coelho, B S Santos, A Fontes, M T S Correia, Quantum dot–cramoll lectin as novel conjugates to glycobiology, J. Photochem. Photobiol. B Biol. 178 (2018) 85–91.
[58] S H Mahadevegowda, S Hou, J Ma, D Keogh, J Zhang, A Mallick, X-W Liu, H Duan, M B Chan-Park, Raman-encoded, multivalent glycan-nanoconjugates for traceable specific binding and killing of bacteria, Biomater. Sci. 6 (2018) 1339–1346.